Manuscript 4959 – Revision 1

Anhydrite stability and the effect of Ca on the behavior of sulfur in felsic magmas

RUIFANG HUANG[1,2] AND HANS KEPPLER[1*]

[1]Bayerisches Geoinstitut, 95440 Bayreuth, Germany

[2]State Key Laboratory of Isotope Geochemistry, Guangzhou Institute of Geochemistry, Chinese Academy of Sciences, 510640 Guangzhou, PR China

* E-mail: Hans.Keppler@uni-bayreuth.de

ABSTRACT

The distribution of sulfur in the system Na_2O-K_2O-CaO-Al_2O_3-SiO_2-H_2O-S was investigated at 2 kbar, 750-950 °C, and oxygen fugacities ranging from the Co-CoO to the Re-ReO_2 buffer. Anhydrite ($CaSO_4$) crystallized in all the experiments conducted at oxidizing conditions (Ni-NiO + 0.5 to 1 and above). Under otherwise equal conditions, an inverse relationship between sulfur and CaO concentration was observed in melts coexisting with anhydrite, with the solubility product $K=[CaO][SO_3]$ being constant, where [CaO] and [SO_3] are the molar fraction of CaO and SO_3 in the quenched glasses. This suggests that anhydrite dissociates upon dissolution in the melt according to $CaSO_{4\ anhydrite} = Ca^{2+}_{melt} + SO_4^{2-}_{melt}$. The solubility product strongly depends on temperature, with $\ln K = -(28573\pm917)/T + (11.26\pm0.80)$. This corresponds to an enthalpy of dissolution of $\Delta H_R = 237.5 \pm 7.6$ kJ/mol. Under reducing conditions (Co-CoO and Ni-NiO buffer), CaO has no effect on the fluid/melt partition coefficient of sulfur $D_S^{fluid/melt}$. At 850 °C, 2 kbar partition coefficients were 519 ± 30 at the Ni-NiO buffer and 516 ± 11 at the Co-CoO buffer, for CaO contents in the melt up to 1 wt. %. These data are virtually identical to those measured in the CaO-free haplogranite system under reducing conditions. However, under more oxidizing conditions, the fluid/melt partition coefficient of sulfur appeared to have increased somewhat in the presence of CaO. This increase may, however, also be related to the fact that the final melt compositions in these runs were distinctly peraluminous. Our data show that calcium has no effect on the degassing of sulfur at reducing conditions, but it greatly reduces the amount of sulfur available for rapid degassing under oxidizing conditions by stabilizing anhydrite.

Keywords: Anhydrite, sulfur, haplogranite, solubility, partitioning, oxygen fugacity

INTRODUCTION

The behavior of sulfur in magmatic-hydrothermal systems has received considerable attention in recent years. Explosive volcanic eruptions may inject large amounts of SO_2 and other sulfur compounds into the atmosphere, where they are photochemically oxidized to sulfate aerosols (McCormick et al. 1995; Robock 2000). These aerosols are believed to be responsible for the global cooling of the atmosphere, which was observed after several recent and historical eruptions (Briffa 1998). Sulfur release from giant flood basalt eruptions may be linked to mass extinction events through the production of acid rain, ocean acidification and resulting anoxia (Black et al. 2014). Measurements of sulfur emissions from active volcanoes are routinely used for the assessment of volcanic hazards (e.g. Duffel et al. 2003; Aiuppa et al. 2007; Oppenheimer et al. 2011). Finally, the formation of some hydrothermal ore deposits is likely closely linked to the behavior of sulfur (e.g. Wilkinson 2013), which may under some circumstances precipitate insoluble sulfides, but which may also facilitate metal transport, e.g. by the formation of hydrosulfide complexes.

Under reducing conditions, the precipitation of pyrrhotite (FeS) often limits the amount of sulfur that may remain in the silicate melt (Baker and Moretti 2011, Parat et al. 2011). At more oxidizing conditions, anhydrite ($CaSO_4$) may crystallize (e.g. Luhr 1984; Bernard et al. 1991), yet the stability of anhydrite has been much less studied than for pyrrhotite (e.g. Carroll and Rutherford 1987; Luhr 1990, 2008; Li and Ripley 2009; Beermann et al. 2011; Parat et al. 2011; Baker and Moretti 2011). Sulfur generally partitions strongly into a hydrous fluid phase coexisting with silicate melts, but fluid/melt partition coefficients reported in the literature vary by orders of magnitude (Scaillet et al. 1998; Keppler 1999, 2010; Botcharnikov et al. 2004; Webster et al. 2009, 2011; Webster and Botcharnikov 2011; Lesne et al. 2011; Zajacz et al. 2012). Most studies now agree that redox state is a prime variable controlling sulfur partitioning and that the fluid/melt partition coefficient increases about one order of magnitude with decreasing oxygen fugacity. Yet, even at the same oxygen fugacity, partition coefficients vary significantly between different studies and it is

not clear whether this variation is real or an experimental artifact and what parameters may control this variation.

The generally strong partitioning of sulfur into a hydrous fluid phase is likely responsible for the "sulfur excess" commonly observed in large explosive volcanic eruptions, i.e. the observation that more sulfur is released in volcanic gases than can be attributed to the degasing of the erupted magma. The most plausible explanation for this phenomenon is that before the eruption, a hydrous fluid coexisted with the silicate melt in the magma chamber and therefore extracted sulfur from a much larger magma reservoir (Wallace and Gerlach 1994; Westrich and Gerlach 1992; Wallace 2001; Keppler 1999, 2010).

As noted above, the behavior of sulfur in magmatic systems is very sensitive to redox conditions, which control the stability of different sulfur species. In silicate melts, sulfur is believed to occur either as sulfide S^{2-} under reducing conditions or as S^{6+} under oxidizing conditions, with the boundary between these two regimes being close to the Ni-NiO buffer (Carroll and Rutherford 1988). H_2S and SO_2 are widely believed to be the most important sulfur species in high-temperature, hydrothermal fluids coexisting with silicate melts, with SO_2 usually being the most important sulfur species in volcanic gases (Fischer 2008). However, recent studies suggest that S^{6+} may become an important sulfur species in hydrous fluids already at moderately oxidizing conditions near the Re-ReO_2 buffer (Binder and Keppler 2011; Ni and Keppler 2012).

In this study, we investigate the behavior of sulfur in a haplogranitic system to which variable amounts of CaO have been added, in order (1) to better understand the factors controlling anhydrite stability and (2) to study the effect of CaO on the partitioning of sulfur between fluid and melt. The haplogranite-CaO system is particularly well suited for these studies, as it is probably the simplest system in which anhydrite stability can be thoroughly studied and the fluid/melt partitioning of sulfur in the CaO-free system is well documented. Keppler (1999) and Keppler (2010) reported fluid/melt partition coefficients of sulfur in this system ranging from 47 under oxidizing to 468 under reducing conditions at 0.5 to 3 kbar and 750 to 850 ˚C.

Very similar partition coefficients, ranging from 50 to 359 were reported by Webster et al. (2011) at 2 kbar and 900 ˚C.

EXPERIMENTAL METHODS

Starting materials and preparation of sample capsules

Starting materials in all experiments were aqueous solutions of H_2SO_4 (0.5 mol/L to 2.5 mol/L) and synthetic haplogranitic glasses with a base composition of 40 wt.% $NaAlSi_3O_8$, 35 wt.% SiO_2, and 25 wt.% $KAlSi_3O_8$, to which up to about 5 wt. % of CaO were added. The solutions were prepared by diluting commercially available standard solutions (Titrisol, Merck). The glasses were prepared from mixtures of high-purity SiO_2, K_2CO_3, Na_2CO_3, Al_2O_3 and $CaCO_3$. The mixtures were decarbonated by heating in an electrical box furnace from ambient temperature to 1100 ºC in 12 hours and annealing at 1100 ºC for 12 hours. The resulting glasses were then re-melted in a high-temperature furnace at 1600 ºC and ambient pressure for two hours. After quenching in distilled water, the glasses were finely ground and homogenized. Glass compositions are given in Table 1.

10 mg H_2SO_4 solution and 10 mg glass powder were sealed into 20 mm long gold capsules with 2.5 mm outer diameter and 0.2 mm wall thickness by arc welding. The amount of H_2SO_4 solution and glass powder added to each charge is listed in Table 2. Capsules were checked for leaks before and after the experiments by heating in an oven at 150 °C for several hours. Capsules that showed any signs of leakage were discarded. A double-capsule technique was used for samples buffered with Re and ReO_2 powder. Around 420 mg buffer mixture (2:1 weight ratio of Re and ReO_2) and 60 mg distilled water were loaded together with the inner capsule into an outer gold capsule with 5.0 mm outer diameter, 0.2 mm wall thickness and 4 cm length.

High-pressure experiments

High-pressure experiments were conducted in vertical rapid-quench cold seal pressure vessels made of the Ni-based super-alloy IN713LC, using water as pressure medium. Sample capsules were mounted on top of a filler rod, which was held in the hot spot of the bomb by means of an external magnet. Run durations were mostly around 7

days. For quenching, the external magnet was dropped, which caused the sample to fall into a water-cooled zone within 1 – 2 s. Temperatures were measured by a Ni-NiCr (type K) thermocouple in an outer drill hole of the autoclave close to the sample position. The accuracy of temperatures is believed to be better than ± 10 °C, including the effects of thermal gradients, as calibrated by internal thermocouples. Pressure was measured with a pressure gauge and is accurate to ± 50 bar or less. The oxygen fugacity inside the vessel was buffered by the reaction of water with the autoclave material, and is 0.5-1 log unit above Ni-NiO. Some experiments were carried out without buffer at the intrinsic oxygen fugacity of the autoclave. For experiments at the Re-ReO_2 buffer, a conventional double capsule technique was used, as described above. For experiments at the Ni-NiO buffer, two sample capsules were placed into an unsealed gold capsule with 5.0 mm outer diameter, 0.2 mm wall thickness and 40 mm length, together with about 0.7 g Ni powder and a trace of NiO. A small gold piece was used to separate the gold capsules from the buffer mixture. For experiments at the Co-CoO buffer, about 0.5 g Co powder was loaded into an unsealed gold capsule with 5.0 mm outer diameter, 0.2 mm wall thickness and ~2 cm length, which was placed below another unsealed gold capsule containing the two sample capsules. These techniques were used to avoid diffusion of Ni or Co into the sample capsule, which does occur if the sample capsules are in direct contact with Ni or Co powder. A few unbuffered experiments at 950 ˚C were carried out in rapid-quench TZM (titanium and zirconium reinforced molybdenum) bombs with argon as pressure medium. The intrinsic oxygen fugacity of these bombs is about 2 log units above Ni-NiO.

Analytical methods

Quenched glasses were analyzed with a JEOL JXA-8900 electron microprobe at 20 kV accelerating voltage, 50 nA beam current, using a defocused beam (20 μm). The peak counting time was 10 s for Na, K and Si, 20 s for Ca and Al and 60 s for S. Albite, orthoclase, enstatite, diopside, and spinel standards were used for analyses of Na, K, Si, Ca and Al, respectively. Due to the use of a defocussed beam, alkali loss during measurement was minimal. Since the position of the SKα line is dependent on the oxidation state of sulfur (Carroll and Rutherford, 1988), both barium sulfate ($BaSO_4$) and zinc sulfide (ZnS) standards were used for S analyses. The SKα position of the samples in this study was located between that of $BaSO_4$ and ZnS. The

difference of the sulfur contents measured using these two standards and their respective peak positions did not exceed the statistical uncertainty.

The valence state of sulfur in the quenched glasses was determined from the wavelength shift of the SKα line as observed by the electron microprobe (Carroll & Rutherford 1988). As suggested by Klimm et al. (2012), measurements were carried out with different exposure times (100 ms, 200 ms, and 300 ms per step) and the observed peak positions were extrapolated to zero exposure time, in order to compensate for changes in oxidation state induced by beam damage. Operating conditions for these measurements were 15 kV, 50 nA, 20 μm defocussed beam, PETH monochromator, scan from 2318 to 2295 eV in 860 steps.

The sulfur content of the fluid phase was calculated by mass balance. In experiments that did not crystallize anhydrite ($CaSO_4$), the sulfur concentration in the fluid was essentially the same as in the starting solution, as only traces of sulfur were found in the quenched glasses and any loss of sulfur to the gold capsule is negligible (Keppler 2010). In experiments that crystallized anhydrite, the amount of sulfur locked up in anhydrite was calculated from the difference in the CaO contents of the quenched glass and the starting glass composition. An implicit assumption in this calculation is that the amount of anhydrite dissolving into the aqueous fluid is negligible. Indeed, Newton and Manning (2005) found a solubility of anhydrite in pure water of 0.03 mol/kg at 10 kbar and 800 ˚C. This would translate into 0.1 wt. % of S in the solution, very small compared to the sulfur contents used in the starting solutions (up to 7 wt. %). For lower pressures and temperatures (500 ˚C and 1 kbar), Moorey and Hesselgesser (1951) reported even lower anhydrite solubilities, equivalent to about $5 \cdot 10^{-4}$ wt. % S in solution.

RESULTS

Run products

The run products of all experiments (Table 2, Fig. 1) contained a quenched glass phase, a quenched fluid phase and usually one crystalline phase, which was anhydrite

$CaSO_4$ at oxidizing conditions (in the unbuffered runs and runs at the Re-ReO_2 buffer) or wollastonite ($CaSiO_3$) at more reducing conditions (Ni-NiO and Co-CoO buffers). The identity of anhydrite and wollastonite was confirmed both by electron microprobe analyses and by Raman spectroscopy. Quenched glasses often contained numerous two-phase fluid inclusions. Raman spectra (Fig. 2) of these fluid inclusions showed that under oxidizing conditions (as defined above), sulfur was mostly present as sulfate SO_4^{2-} in the liquid phase, while for experiments at reducing conditions, H_2S was detected both in the liquid and the gas phase. This is consistent with the strong smell of H_2S that was often noticed when opening capsules from reduced experiments; a slight odor of SO_2 was sometimes noticed for the experiments that had been run without buffer (i.e. 0.5 to 1 log unit above Ni-NiO). The pH of the quenched fluid, as measured by a pH indicator paper, was 0.5 for the oxidized runs and 10 for the reduced runs. The compositions of quenched silicate glasses are compiled in Table 3. Glass compositions were always found to be homogeneous, indicating attainment of equilibrium. Due to the crystallization of anhydrite and wollastonite, measured CaO contents were lower than in the starting materials, 0.05 to 1.19 wt.% for runs with anhydrite and 0.88 – 1.28 wt.% for runs with wollastonite. Due to the partitioning of alkalis into the fluid, the glasses from experiments at oxygen fugacities above Ni-NiO became distinctly peraluminous, with molar $Al_2O_3/(CaO + Na_2O + K_2O)$ ratios usually ranging between 1.1 and 1.2. For the run products from experiments at the Ni-NiO and the Co-CoO buffer, this ratio was usually slightly below 1. For unbuffered runs 0.5 to 1 log unit above the Ni-NiO buffer, a S^{6+}/S_{total} ratio of 0.83 was observed in the quenched glasses, while for the runs conducted in TZM bombs about 2 log units above Ni-NiO, the ratio was 0.90.

Stability of anhydrite

In principle, anhydrite could dissolve in the silicate melt in two different ways. If there were some strong association between SO_3 and CaO in the melt, forming some kind of molecule-like unit, the dissolution may be described by the equation

$$CaSO_4 \text{ (crystal)} = CaSO_4 \text{ (melt)}$$

However, if calcium and sulfur dissociate in the melt, the dissolution could be described by

$$CaSO_4 \text{ (crystal)} = Ca^{2+} \text{ (melt)} + SO_4^{2-} \text{ (melt)}$$

or

$$CaSO_4 \text{ (crystal)} = CaO \text{ (melt)} + SO_3 \text{ (melt)}$$

For the first case, the solubility of anhydrite is independent on the CaO content of the melt, while it is dependent on the CaO content of the melt if dissociation occurs. The SO_3 content of the quenched glasses correlates negatively with the CaO content (Fig. 3), while the solubility product of anhydrite in the melt is constant for experiments conducted at the same temperature and pressure (Fig. 4). The solubility product of anhydrite can be expressed as

$$K = [CaO][SO_3]$$

where [CaO] and [SO_3] are molar fractions of CaO and SO_3 in the quenched glasses, respectively. Molar fractions were calculated on an anhydrous base, from converting analyses of quenched glasses into oxide components of SiO_2, Al_2O_3,CaO, Na_2O, K_2O and SO_3. The concentration of SO_3 in the melt was calculated from the bulk sulfur contents of the glasses in Table 3 and the S^{6+}/S_{total} ratio (see above). Thus, anhydrite dissolves in the melt by dissociating into Ca^{2+} and SO_4^{2-} or into CaO and SO_3; the latter two cases cannot be distinguished from a thermodynamic point of view. Figure 5 shows the temperature dependence of anhydrite solubility in the melt as a plot of lnK versus inverse temperature. All data can be described by one single regression line

$$\ln K = (11.26 \pm 0.80) - (28573 \pm 917)/T$$

($R^2 = 0.92$), where T is temperature in Kelvin. According to $d\ln K/d(1/T) = -\Delta H/R$, his corresponds to a reaction enthalpy of $\Delta H_R = 237.5 \pm 7.6$ kJ/mol. If the solubility product is expressed in wt. % CaO and SO_3 of the hydrous glasses, linear regression of the data yields

$$\ln K(\text{wt.}\%) = (19.5 \pm 1.4) - (27372 \pm 1635)/T$$

Only the data at 750 ˚C plot somewhat above these regression lines, which could imply incomplete crystallization of anhydrite at these relatively low temperatures.

The observation of a constant solubility product of anhydrite at high oxygen fugacities and constant pressure and temperature reported here is similar to the solubility behavior of fluorite CaF_2 in haplogranitic melts, as observed by Dolejs and Baker (2006).

Fluid/melt partitioning of sulfur under reduced conditions

Data on the partitioning of sulfur between silicate melt and aqueous fluid at 850 ˚C and 2 kbar are compiled in Table 4. At reducing conditions (i.e. at the Co-CoO and the Ni-NiO buffer), wollastonite crystallized. This caused the CaO content in the glasses to be nearly constant around 1 wt. % (Table 2), independent of the bulk CaO content in the starting material, as all runs were carried out at the same pressure and temperature (2 kbar and 850 ˚C). As no sulfur-bearing phase crystallized in these runs and as the sulfur contents in the glasses are very low, the equilibrium sulfur concentration in the fluid is essentially the same as for the starting solution. Figure 6 shows a plot of the sulfur content in the melt versus the sulfur content in the fluid for all experiments at the Co-CoO buffer. All data points follow a straight line through the origin of the diagram, implying that the fluid/melt partition coefficient is independent of sulfur concentration; linear regression yielded $D_s^{fluid/melt} = 509 \pm 20$. Figure 7 shows similar data for Ni-NiO buffer conditions. Again, the fluid/melt partitioning of sulfur can be described by one single partition coefficient $D_s^{fluid/melt} = 505 \pm 19$. The close agreement between the partition coefficients found for Ni-NiO and Co-CoO buffer conditions implies that sulfur speciation in melt and fluid does not change in this range of oxygen fugacity. Indeed, Raman measurements of quenched aqueous fluids (Binder and Keppler 2011) and the sulfur Kα shift of quenched glasses (Carroll and Rutherford 1988) suggest the prevalence of S^{2-} at these conditions. Moreover, the data obtained here for melts containing about 1 wt. % of CaO in equilibrium with wollasonite are within the combined errors indistinguishable from the partition coefficients of sulfur ($D_s^{fluid/melt} = 468 \pm 32$) in the Ca-free haplogranite system at the Co-CoO buffer under otherwise equal conditions (Keppler 1999, 2010). This suggests that CaO has no effect on the fluid/melt partitioning of sulfur under

reducing conditions and S^{2-} or H_2S do not form any close association with Ca in either the fluid or the silicate melt.

Fluid/melt partitioning of sulfur under oxidizing conditions

In unbuffered runs (0.5 to 1 log unit above the Ni-NiO buffer), the crystallization of anhydrite reduced the initial CaO content in the melt. The resulting quenched glasses mostly have CaO contents between 0.05 and 0.3 wt.%. In order to better separate out the effect of CaO on the behavior of sulfur, the data were divided into two groups, one with a CaO content in the quenched melt below 0.2 wt. % and one with CaO above 0.2 wt. %. Figure 8 shows the sulfur partitioning for experiments with melt CaO contents below 0.2 wt. %. Although there clearly is some scatter, possibly related to variations in CaO content, the data can still be reasonably described by a constant partition coefficient of $D_s^{fluid/melt} = 104 \pm 13$. This value is, however, already significantly higher than the partition coefficient of 47 ± 4 found by Keppler (2010) for the CaO-free haplogranite system under otherwise equal conditions. A further increase of partition coefficients is obvious in the data for melts with a CaO content of more than 0.2 wt. % (Fig. 9), with $D_s^{fluid/melt}$ exceeding 200 for high sulfur concentrations in the fluid. However, the data also suggest that that the partition coefficient is not constant, but increases with the sulfur content in the fluid. The data from four experiments at the Re-ReO_2 buffer (Fig. 10) can be described by a constant partition coefficient of $D_s^{fluid/melt} = 157 \pm 15$, similar to the values measured in the unbuffered experiments. Figure 11 shows a comparison of the sulfur partition coefficients measured in this study and of those in the CaO-free haplogranite system (Keppler 2010).

A conceivable explanation for the effect of Ca on the partitioning of sulfur could be the formation of ion pairs between Ca^{2+} and the sulfur species in the fluid. However, the very low solubility of anhydrite in water (Morey and Hesselgesser 1951, Newton and Manning 2005) makes it questionable, whether the Ca^{2+} concentration in the fluid is high enough for such an effect. Indirect effects, such as changes in the pH of the fluid upon addition of excess CaO to the system, or changes in the partitioning of Na and K upon addition of Ca, could also be involved. Moreover, the data shown in Figure 9 may imply that at high Ca concentrations, there is significant non-ideality in the sulfur-rich aqueous fluids coexisting with the silicate melts, as the sulfur content

in the melt increases only slightly with the sulfur content in the fluid. The apparent increase of the fluid/melt partition coefficient of sulfur in the presence of CaO cannot be a caused by errors in the mass balance calculation. The main assumption here is that the solubility of anhydrite in the fluid is negligible, in line with experimental studies by Moorey and Hesselgesser (1951) and Newton and Manning (2005). However, if one allowed some solubility of anhydrite in the fluid, this would only increase the sulfur concentration in the fluid and therefore further increase the fluid/melt partition coefficient. It is conceivable, however, that the fluid/melt partition coefficient is influenced by the distinctly peraluminous composition of the melts in these experiments. Indeed, Binder (2007) found that in the CaO-free haplogranite system, the fluid melt partition coefficient of sulfur increases from 74 ± 5 to 246 ± 9 when $Al_2O_3/(Na_2O+K_2O)$ rises from 0.93 to 1.18 (at 2 kbar, 850 ˚C and the Re-ReO_2 buffer). A similar effect could be responsible for the apparent increase of the fluid/melt partition coefficient with CaO content observed here.

THE EFFECT OF CA ON THE DEGASSING OF SULFUR

Our study clearly shows that the presence of calcium does not affect the behavior of sulfur at all if oxygen fugacity is low (Ni-NiO or below). No sulfur-bearing phases are being stabilized and the fluid/melt partition coefficient of sulfur remains unaffected. However, already small amounts of calcium have a major effect on sulfur under more oxidizing conditions, because on one hand, part of the sulfur is locked up by the crystallization of anhydrite, while on the other hand, the fluid/melt partition coefficient of the remaining sulfur possibly increases. Obviously, these two effects would tend to act in the opposite direction on the sulfur yield in volcanic eruptions. Increasing the fluid/melt partition coefficient should increase the amount of sulfur entering the fluid phase, while locking up sulfur in anhydrite should reduce it. Here, we will argue that the second effect is much more important and that the main effect of calcium is to reduce the sulfur yield of explosive eruptions. This conclusion depends very much on the stability of anhydrite during an eruption.

Kinetic data on the decomposition of anhydrite (Hanic et al. 1985) suggest that during the short timescales of explosive eruptions, very little sulfur may be released by decomposition of anhydrite. At 1310 ˚C, far above the expected eruption temperature,

10 % decomposition requires more than 3 hours. This is consistent with the fresh appearance of anhydrite phenocrysts in Mt. Pinatubo pumices (Bernard et al. 1991; see also Wallace and Gerlach 1994 for further discussion). With the assumption that sulfur in anhydrite is not available for release into the gas phase during an eruption, the sulfur yield can readily be calculated. Figure 12 shows such model calculations for a magmatic system with rhyolitic composition under oxidizing conditions and a bulk sulfur content of 1000 ppm S, equivalent to 0.25 wt. % of SO_3. This value is comparable to the SO_3 content in whole-rock pumices from the 1991 Mt. Pinatubo eruption (0.37 – 0.48 wt. %; Bernard et al. 1991), but smaller than for El Chicón (1.2 wt. %, Luhr et al. 1984). In the calculations, it was assumed that all sulfur in the melt is in the S^{6+} state and that the sulfur concentration in the melt is controlled by the solubility product of anhydrite. Figure 12 shows clearly that the main effect of CaO is to precipitate anhydrite and thereby to greatly reduce the fraction of the total sulfur that enters the fluid phase. Increasing the fluid/melt partition coefficient would only slightly reduce this effect.

Our data therefore show that CaO is a main factor in controlling the sulfur yield of explosive eruptions under oxidizing conditions. For rhyolitic compositions, the data on anhydrite solubility presented here can be directly applied. However, for dacitic and andesitic compositions, independent calibrations are required as the solubility product likely also depends on the bulk composition of the melt. Indeed, the data of Luhr et al. (1990) suggest that for more depolymerized melts, the solubility of anhydrite increases. Empirical models for anhydrite solubility have been proposed by Li and Ripley (2009) and by Baker and Moretti (2011). The latter model does include a term with the molar fraction of CaO. However, the exponent of this CaO term in the equation of sulfur solubility of Baker and Moretti (2001) is only –0.21, not –1, as one would expect from the constancy of the solubility product. Very likely, two effects are mixed here: On one hand, CaO reduces the solubility of S in the melt according to the solubility product, which should remain constant at given bulk composition, pressure and temperature, as shown in this study. However, CaO may also act as a network modifier that depolymerizes the melt, an effect that likely increases the solubility product. We therefore suggest that models of anhydrite solubility may require some recalibration, which fit the solubility product as a function of pressure, temperature

and some compositional parameter, such as NBO/T (non-bridging oxygen per tetrahedron).

ACKNOWLEDGEMENTS

We would like to thank Roman Botcharnikov and an anonymous referee for constructive reviews and Nicole Métrich for the editorial handling of the manuscript.

REFERENCES CITED

Aiuppa, A., Moretti, R., Federico, C., Giudice, G., Gurrieri, S., Liuzzo, M., Papale, P., Shinohara, H., and Valenza, M. (2007) Forecasting Etna eruptions by real-time observation of volcanic gas composition. Geology, 35, 1115-1118.

Baker, D.R., and Moretti, R. (2011) Modeling the solubility of sulfur in magmas: A 50-year old geochemical challenge. Reviews in Mineralogy and Geochemistry, 73, 167-213.

Beermann, O., Botcharnikov, R.E., Holtz, F., Diedrich, O., and Nowak, M. (2011) Temperature dependence of sulfide and sulfate solubility in olivine-saturated basaltic magmas. Geochimica et Cosmochimica Acta, 75, 7612-7631,

Bernard, A., Demaiffe, D., Mattielli, N., and Punongbayan, R. S. (1991) Anhydrite-bearing pumices from Mount Pinatubo: further evidence for the existence of sulfur-rich silicic magmas. Nature, 354, 139-140.

Binder, B. (2007) Experimentelle Untersuchungen zum Verhalten von Schwefel in magmatisch-hydrothermalen Systemen. Ph. D. dissertation, University of Tübingen.

Binder, B., and Keppler, H. (2011) The oxidation state of sulfur in magmatic fluids. Earth and Planetary Science Letters, 301, 190-198.

Black, B.A., Lamarque, J.F., Shields, C.A., Elkins-Tanton, L.T., and Kiehl, J.T. (2014) Acid rain and ozone depletion from pulsed Siberian Traps magmatism. Geology, 42, 67-70.

Botcharnikov, R. E., Behrens, H., Holtz, F., Koepke, J., and Sato, H. (2004) Sulfur and chlorine solubility in Mt. Unzen rhyodacitic melt at 850 °C and 200 MPa. Chemical Geology, 213, 207-225.

Briffa, K. R., Jones, P. D., and Schweingruber, F. H. (1998) Influence of volcanic eruptions on Northern Hemisphere summer temperature over the past 600 years. Nature, 393, 450-455.

Carroll, M. R., and Rutherford, M. J. (1987) The stability of igneous anhydrite: Experimental results and implications for sulfur behavior in the 1982 El Chichon trachyandesite and other evolved magmas. Journal of Petrology, 28, 781-801.

Carroll, M. R., and Rutherford, M. J. (1988) Sulfur speciation in hydrous experimental glasses of varying oxidation state: Results from measured wavelength shifts of sulfur X-rays. American Mineralogist, 73, 845-849.

Dolejs, D., and Baker, D.R .(2006) Fluorite solubility in hydrous haplogranitic melts at 100 MPa. Chemical Geology, 225, 40-60.

Duffell, H. J., Oppenheimer, C., Pyle, D. M., Galle, B., McGonigle, A. J. S., and Burton, M. R. (2003) Changes in gas composition prior to a minor explosive eruption at Masays volcano, Nicaragua. Journal of Volcanology and Geothermal Research, 126, 327-339.

Fischer, T. P. (2008) Fluxes of volatiles (H_2O, CO_2, N_2, Cl, F) from arc volcanoes. Geochemical Journal, 42, 21-38.

Hanic, F., Galikova, L., Havlica, J., Kapralik, I., and Ambruz, V. (1985) Kinetics of the thermal decomposition of $CaSO_4$ in air. British Ceramics Transactions and Journal, 84, 22-25.

Keppler, H. (1999) Experimental evidence for the source of excess sulfur in explosive volcanic eruptions. Science, 284, 1652-1654.

Keppler, H. (2010) The distribution of sulfur between haplogranitic melts and aqueous fluids. Geochimica et Cosmochimica Acta, 74, 645-660.

Klimm, K., Kohn, S.C., O'Dell L.A., Botcharnikov, R.E., and Smith, M.E. (2012) The dissolution mechanism of sulphur in hydrous silicate melts. I: Assessment of analytical techniques in determining the sulphur speciation in iron-free to iron-poor glasses. Chemical Geology, 322-323, 237-249.

Lesne, P., Kohn, S. C., Blundy, J., Witham, F., Botcharnikov, R. E., and Behrens, H. (2011) Experimental simulation of closed-system degassing in the system basalt-H_2O-CO_2-S-Cl. Journal of Petrology, 52, 1737-1762.

Li, C.S., and Ripley, E.M (2009) Sulfur contents at sulfide-liquid or anhydrite saturation in silicate melts: Empirical equations and example applications. Economic Geology, 104, 405-412.

Luhr, J. F., Carmichael, I. S. E., and Varekamp, J. C. (1984) The 1982 eruptions of El Chichón volcano, Chiapas, Mexico: Mineralogy and petrology of the anhydrite-bearing pumices. Journal of Volcanology and Geothermal Research, 23, 69-108.

Luhr, J. F. (1990) Experimental phase relations of water- and sulfur-saturated arc magmas and the 1982 eruptions of El Chichon volcano. Journal of Petrology, 31, 1071-1114.

Luhr, J. F. (2008) Primary igneous anhydrite: Progress since its recognition in the 1982 El Chichon trachyandesite. Journal of Volcanology and Geothermal Research, 175, 394-407.

McCormick, M. P., Thomason, L. M., and Trepte, C. R. (1995) Atmospheric effects of the Mt Pinatubo eruption. Nature, 373, 399-404.

Moorey, G.W., and Hesselgesser, J.M. (1951) The solubility of some minerals in superheated steam at high pressures. Economic Geology, 46, 821-835.

Newton, R.C., and Manning, C.E. (2005) Solubility of anhydrite, $CaSO_4$, in NaCl-H_2O solutions at high pressures and temperatures: Applications to fluid-rock interaction. Journal of Petrology, 46, 701-716.

Ni, H. W., and Keppler, H. (2012) In-situ Raman spectroscopic study of sulfur speciation in oxidized magmatic-hydrothermal fluids. American Mineralogist, 97, 1348-1353.

Oppenheimer, C., Scaillet, B. and Martin, R. S. (2011) Sulfur degassing from volcanoes: Source conditions, surveillance, plume chemistry and earth system impacts. Reviews in Mineralogy and Geochemistry, 73, 363-421.

Parat, F., Holtz, F., Streck, M.J. (2011) Sulfur-bearing magmatic accessory minerals. Reviews in Mineralogy and Geochemistry, 73, 285-314.

Robock, A. (2000) Volcanic eruptions and climate. Reviews of Geophysics, 38, 191-219.

Scaillet, B., Clemente, B., Evans, B. W., and Pichavant, M. (1998) Redox control of sulfur degassing in silicic magmas. Journal of Geophysical Research, 103, 23937-23949.

Wallace, P. J. (2001) Volcanic SO_2 emissions and the abundance and distribution of exsolved gas in magma bodies. Journal of Volcanology and Geothermal Research, 108, 85-106.

Wallace, P. J., and Gerlach, T. M. (1994) Magmatic vapor source for sulfur dioxide released during volcanic eruptions: Evidence from Mount Pinatubo. Science, 265, 497-499.

Webster, J.D., and Botcharnikov, R.E. (2011) Distribution of sulfur between melt and fluid in S-O-H-C-Cl-bearing magmatic systems at shallow crustal pressures and temperatures. Reviews in Mineralogy and Geochemistry, 73, 247-283.

Webster, J. D., Sintoni, M. F., and de Vivo B. (2009) The partitioning behavior of Cl, S, and H_2O in aqueous vapor- ±saline-liquid saturated phonolitic and trachytic melts at 200 MPa. Chemical Geology, 263, 19-36.

Webster, J. D., Goldoff, B., and Shimizu, N. (2011) C-O-H-S fluids and granitic magma: How S partitions and modifies CO_2 concentrations of fluid-saturated felsic melt at 200 MPa. Contributions to Mineralogy and Petrology, 162, 849-865.

Westrich, H. R., and Gerlach, T. M. (1992) Magmatic gas source for the stratospheric SO_2 cloud from the June 15, 1991, eruption of Mount Pinatubo. Geology, 20, 867-870.

Wilkinson, J.T. (2013) Triggers for the formation of porphyry ore deposits in magmatic arcs. Nature Geoscience, 6, 917-925.

Zajacz, Z., Candela, P. A., Piccoli, P. M., and Sanchez-Valle, C. (2012) The partitioning of sulfur and chlorine between andesite melts and magmatic volatiles and the exchange coefficients of major cations. Geochimica et Cosmochimica Acta, 89, 81-101.

TABLE 1. Compositions of glasses used as starting materials (in wt. %)

	Glass 1	Glass 2	Glass 3	Glass 4	Glass 5
SiO_2	76.58(48)	75.86(33)	75.92(41)	74.21(57)	73.69(39)
CaO	0.84(05)	2.01(04)	2.78(07)	3.98(12)	4.79(07)
Na_2O	4.60(14)	4.71(10)	4.54(09)	4.65(13)	4.44(09)
K_2O	4.15(07)	4.14(12)	3.99(08)	4.08(9)	3.95(06)
Al_2O_3	12.61(30)	12.35(13)	12.43(23)	12.15(28)	11.99(05)
Total	98.78(33)	99.08(35)	99.65(28)	99.08(25)	98.85(41)

Notes. Compositions were determined by electron microprobe. Numbers in brackets are one standard deviation

TABLE 2. Summary of hydrothermal experiments

Sample No.	T (°C)	P (kbar)	Oxygen fugacity	Bulk CaO (wt.%)	Glass (mg)	H_2SO_4 (M)	Solution (mg)	Run duration (days)	Run products*
HR64	750	2	Ni-NiO + 0.5	2.01	10.31	0.5	10.5	10	Gl, Fl, An
HR65	750	2	Ni-NiO + 0.5	2.79	10.5	0.5	10.49	10	Gl, Fl, An
HR10	850	2	Ni-NiO + 0.5	0.85	10.48	0.5	9.85	11	Gl, Fl, An
HR18	850	2	Ni-NiO + 0.5	0.85	11.02	1	10.52	9	Gl, Fl, An
HR01	850	2	Ni-NiO + 0.5	0.85	10.17	1.5	11.24	9	Gl, Fl, An
HR08	850	2	Ni-NiO + 0.5	0.85	10.28	2	11.22	7	Gl, Fl, An
HR03	850	2	Ni-NiO + 0.5	0.85	10.43	2.5	11.79	10	Gl, Fl, An
HR19	850	2	Ni-NiO + 0.5	2.01	10.32	0.5	10.34	9	Gl, Fl, An
HR17	850	2	Ni-NiO + 0.5	2.01	10.95	1	10.65	9	Gl, Fl, An
HR29	850	2	Ni-NiO + 0.5	2.01	11.37	1.5	10.18	6	Gl, Fl, An
HR20	850	2	Ni-NiO + 0.5	2.01	11.00	2	10.82	8	Gl, Fl, An
HR84	850	2	Ni-NiO + 0.5	2.01	10.10	2	11.00	6	Gl, Fl, An
HR79	850	2	Ni-NiO + 0.5	2.01	10.68	2.5	11.36	9	Gl, Fl, An
HR05	850	2	Ni-NiO + 0.5	2.01	10.45	2.5	11.81	9	Gl, Fl, An
HR30	850	2	Ni-NiO + 0.5	2.79	10.76	1	9.51	6	Gl, Fl, An
HR16	850	2	Ni-NiO + 0.5	2.79	10.91	1.5	10.82	9	Gl, Fl, An
HR21	850	2	Ni-NiO + 0.5	2.79	10.76	2	11.15	8	Gl, Fl, An
HR85	850	2	Ni-NiO + 0.5	2.79	10.46	2	10.86	6	Gl, Fl, An
HR80	850	2	Ni-NiO + 0.5	2.79	10.86	2.5	11.21	9	Gl, Fl, An
HR06	850	2	Ni-NiO + 0.5	2.79	10.39	2.5	11.68	9	Gl, Fl, An
HR09	850	2	Ni-NiO + 0.5	4.85	10.33	0.5	10.13	11	Gl, Fl, An
HR02	850	2	Ni-NiO + 0.5	4.85	10.44	1.5	11.08	9	Gl, Fl, An
HR07	850	2	Ni-NiO + 0.5	4.85	10.28	2	11.08	7	Gl, Fl, An
HR04	850	2	Ni-NiO + 0.5	4.85	10.46	2.5	11.63	10	Gl, Fl, An
HR60	850	2	Re-ReO_2	0.85	10.71	0.5	10.74	6	Gl, Fl, An
HR73	850	2	Re-ReO_2	0.85	11.68	2	11.72	6	Gl, Fl, An
HR81	850	2	Re-ReO_2	2.01	10.55	0.5	10.56	6	Gl, Fl, An
HR82	850	2	Re-ReO_2	2.79	10.65	0.5	10.57	5	Gl, Fl, An
HR22	950	2	Ni-NiO +2	0.85	10.17	0.5	9.84	6	Gl, Fl, An
HR24	950	2	Ni-NiO +2	0.85	10.74	1	10.51	6	Gl, Fl, An
HR13	950	2	Ni-NiO + 2	0.85	11.32	1.5	10.13	7	Gl, Fl, An
HR11	950	2	Ni-NiO + 2	0.85	10.48	2.5	11.52	7	Gl, Fl, An
HR12	950	2	Ni-NiO +2	4.85	10.9	2.5	11.44	7	Gl, Fl, An
HR14	890	2	Ni-NiO + 0.5	2.79	10.61	0.5	10.27	7	Gl, Fl, An
HR15	890	2	Ni-NiO + 0.5	0.85	10.84	0.5	9.7	7	Gl, Fl, An
HR31	850	2	Ni-NiO	0.85	11.10	0.5	10.50	6	Gl, Fl,Wo
HR36	850	2	Ni-NiO	0.85	10.69	1	10.58	6	Gl, Fl, Wo
HR27	850	2	Ni-NiO	0.85	10.80	1.5	10.50	6	Gl, Fl, Wo
HR34	850	2	Ni-NiO	0.85	10.23	2	10.98	6	Gl, Fl, Wo

HR66	850	2	Ni-NiO	0.85	11.06	2.5	11.45	6	Gl, Fl, Wo
HR32	850	2	Ni-NiO	2.01	10.87	0.5	10.41	6	Gl, Fl, Wo
HR83	850	2	Ni-NiO	2.01	10.32	0.5	10.00	7	Gl, Fl, Wo
HR25	850	2	Ni-NiO	2.01	11.2	1	10.7	6	Gl, Fl, Wo
HR54	850	2	Ni-NiO	2.01	10.57	1	10.42	6	Gl, Fl, Wo
HR28	850	2	Ni-NiO	2.01	10.29	1.5	10.90	6	Gl, Fl, Wo
HR35	850	2	Ni-NiO	2.01	10.43	2	11.15	6	Gl, Fl, Wo
HR67	850	2	Ni-NiO	2.01	10.56	2.5	11.46	6	Gl, Fl, Wo
HR33	850	2	Ni-NiO	2.79	10.49	0.5	10.31	6	Gl, Fl, Wo
HR26	850	2	Ni-NiO	2.79	10.59	1	10.42	6	Gl, Fl, Wo
HR55	850	2	Ni-NiO	2.79	10.65	1	10.53	6	Gl, Fl, Wo
HR39	850	2	Ni-NiO	2.79	10.49	1.5	10.97	6	Gl, Fl, Wo
HR68	850	2	Ni-NiO	2.79	11.45	2.5	11.37	6	Gl, Fl, Wo
HR37	850	2	Ni-NiO	4.02	10.04	1	9.61	6	Gl, Fl, Wo
HR40	850	2	Ni-NiO	4.02	11.50	1.5	11.04	6	Gl, Fl, Wo
HR43	850	2	Ni-NiO	4.02	11.29	2	11.61	7	Gl, Fl, Wo
HR69	850	2	Ni-NiO	4.02	10.75	2.5	11.27	6	Gl, Fl, Wo
HR38	850	2	Ni-NiO	4.85	10.28	1	10.36	6	Gl, Fl, Wo
HR41	850	2	Ni-NiO	4.85	10.22	1.5	10.70	7	Gl, Fl, Wo
HR44	850	2	Ni-NiO	4.85	10.60	2	11.11	7	Gl, Fl, Wo
HR62	850	2	Co-CoO	0.85	10.1	1	10.89	6	Gl, Fl, Wo
HR70	850	2	Co-CoO	0.85	10.74	1.5	11.39	6	Gl, Fl, Wo
HR75	850	2	Co-CoO	0.85	10.28	2	11.14	6	Gl, Fl, Wo
HR77	850	2	Co-CoO	0.85	10.17	2.5	11.36	6	Gl, Fl, Wo
HR61	850	2	Co-CoO	2.01	10.73	0.5	10.47	6	Gl, Fl, Wo
HR71	850	2	Co-CoO	2.01	10.25	1.5	11.44	6	Gl, Fl, Wo
HR76	850	2	Co-CoO	2.01	10.06	2	11.55	6	Gl, Fl, Wo
HR78	850	2	Co-CoO	2.01	10.32	2.5	11.93	6	Gl, Fl, Wo

Notes: *Gl: glass, Fl: fluid, An: anhydrite, Wo: wollastonite. The glasses used as starting material are identified by their CaO content; for full compositions, see Table 1.

Table 3. Composition of silicate glasses from hydrothermal experiments (in wt.%)

	n*	SiO_2	Al_2O_3	CaO	Na_2O	K_2O	S	Total	A/NK**	A/CNK§
HR64	25	72.22(22)	11.95(13)	0.14(1)	3.57(9)	3.87(6)	0.0062(11)	91.77(32)	1.19	1.16
HR65	24	71.85(18)	11.91(11)	0.50(3)	3.62(5)	3.90(4)	0.0032(8)	91.80(19)	1.17	1.07
HR10	9	71.98(41)	12.63(22)	0.28(1)	4.01(14)	3.99(5)	0.014(1)	92.93(27)	1.2	1.11
HR18	15	73.67(25)	12.10(6)	0.102(4)	3.88(10)	3.78(4)	0.026(1)	93.60(35)	1.16	1.14
HR01	9	71.83(17)	11.91(5)	0.14(1)	4.01(5)	3.90(3)	0.019(1)	91.83(22)	1.1	1.08
HR08	10	72.95(40)	12.01(13)	0.23(1)	3.92(21)	3.87(6)	0.015(1)	93.03(57)	1.13	1.09
HR03	12	71.44(35)	12.39(19)	0.16(1)	4.23(8)	3.99(2)	0.021(1)	92.27(27)	1.1	1.07
HR19	14	73.65(22)	12.07(4)	0.26(1)	3.92(8)	3.79(5)	0.010(1)	93.71(29)	1.14	1.09
HR17	16	72.52(35)	11.97(6)	0.17(1)	3.63(13)	3.90(4)	0.015(2)	92.24(50)	1.17	1.14
HR29	35	72.99(48)	12.05(28)	0.084(9)	3.92(16)	3.83(6)	0.035(3)	92.95(29)	1.14	1.12
HR20	21	73.15(31)	11.85(12)	0.05(1)	3.43(18)	3.75(14)	0.066(5)	92.34(39)	1.22	1.21
HR84	20	72.98(39)	12.01(7)	0.092(6)	3.78(6)	3.81(3)	0.031(2)	92.77(42)	1.16	1.14
HR79	19	72.23(85)	12.20(59)	0.090(15)	3.66(22)	3.85(12)	0.038(4)	92.10(35)	1.2	1.18
HR05	12	72.94(42)	12.09(26)	0.22(2)	3.98(10)	3.90(5)	0.015(1)	93.17(30)	1.12	1.08
HR30	23	73.10(26)	12.02(11)	0.14(1)	3.93(6)	3.87(3)	0.019(1)	93.10(23)	1.13	1.10
HR16	15	72.35(17)	11.87(4)	0.16(1)	3.50(18)	3.93(12)	0.018(1)	91.86(21)	1.19	1.15
HR21	24	72.55(82)	12.04(37)	0.055(8)	3.27(21)	3.88(13)	0.064(5)	91.92(53)	1.26	1.24
HR85	21	72.99(40)	12.06(6)	0.095(6)	3.74(7)	3.86(5)	0.031(3)	92.80(45)	1.17	1.15
HR80	26	72.92(37)	12.04(18)	0.085(7)	3.58(11)	3.86(6)	0.035(2)	92.58(39)	1.2	1.18
HR06	10	72.97(31)	12.15(8)	0.067(5)	3.92(5)	3.87(3)	0.045(2)	93.09(32)	1.14	1.13
HR09	10	70.99(14)	12.19(3)	1.19(5)	3.85(4)	3.90(3)	0.013(1)	92.16(21)	1.15	0.96
HR02	10	71.88(37)	11.93(7)	0.24(8)	3.99(7)	3.90(5)	0.013(1)	91.99(25)	1.11	1.06
HR07	10	72.78(24)	12.05(6)	0.27(1)	4.00(7)	3.84(6)	0.013(1)	92.98(34)	1.12	1.07
HR04	11	70.86(26)	12.14(6)	0.24(1)	3.67(31)	3.98(9)	0.018(6)	90.93(27)	1.17	1.13
HR60	15	72.30(25)	12.11(15)	0.20(1)	3.90(10)	3.98(7)	0.013(1)	92.50(40)	1.13	1.09
HR73	20	72.53(80)	12.34(48)	0.13(1)	3.92(18)	3.92(9)	0.032(4)	92.92(43)	1.15	1.13
HR81	19	72.64(39)	12.06(14)	0.30(1)	3.83(8)	3.86(4)	0.010(2)	92.72(36)	1.15	1.09
HR82	20	72.81(35)	12.14(9)	0.50(2)	3.92(8)	3.87(4)	0.0062(9)	93.26(40)	1.14	1.05
HR22	16	72.74(23)	12.36(5)	0.160(5)	3.52(4)	3.70(2)	0.122(4)	92.54(25)	1.26	1.23
HR24	23	73.45(17)	12.24(5)	0.095(4)	3.05(16)	3.07(3)	0.350(34)	92.50(34)	1.47	1.44
HR13	15	74.14(30)	11.93(4)	0.091(1)	2.80(4)	2.94(2)	0.42(3)	92.95(20)	1.53	1.50
HR11	8	81.29(14)	7.83(8)	0.051(4)	1.48(4)	1.71(2)	0.41(1)	93.39(8)	1.83	1.79
HR12	11	77.07(25)	10.07(13)	0.067(6)	2.16(6)	2.37(3)	0.46(2)	92.89(11)	1.65	1.61
HR14	12	72.06(27)	11.93(5)	0.68(1)	3.75(6)	3.89(2)	0.012(1)	92.34(36)	1.15	1.03
HR15	14	73.01(33)	12.18(12)	0.21(1)	3.90(6)	3.88(5)	0.019(2)	93.23(28)	1.15	1.11
HR31	22	72.19(33)	12.95(45)	0.90(2)	4.05(19)	3.91(4)	0.0051(12)	94.00(36)	1.19	1.03
HR36	21	71.02(65)	12.31(34)	0.88(4)	4.29(13)	3.97(6)	0.0082(19)	92.56(26)	1.08	0.95
HR27	23	72.78(25)	11.83(7)	0.89(3)	3.95(29)	3.85(3)	0.0099(10)	93.32(24)	1.11	0.96
HR34	24	72.60(30)	12.81(32)	0.90(2)	3.99(28)	3.88(3)	0.010(1)	94.20(42)	1.19	1.03
HR66	25	72.80(25)	12.01(17)	0.88(2)	4.03(6)	3.89(4)	0.010(1)	93.64(21)	1.11	0.97
HR32	25	72.06(32)	13.08(39)	0.98(2)	4.09(25)	3.98(3)	0.0042(9)	94.19(44)	1.19	1.02
HR83	20	72.12(41)	12.17(6)	1.02(1)	3.94(7)	3.89(3)	0.0044(14)	93.17(48)	1.14	0.97
HR25	22	72.29(19)	11.91(6)	1.00(2)	4.07(6)	3.86(3)	0.0075(18)	93.13(24)	1.1	0.94

HR54	25	72.35(52)	12.07(5)	1.02(1)	4.07(6)	3.89(4)	0.0065(15)	93.42(60)	1.11	0.95
HR28	24	72.37(33)	12.01(20)	1.00(3)	4.09(13)	3.87(4)	0.012(1)	93.37(22)	1.1	0.94
HR35	23	71.43(32)	12.04(13)	1.06(4)	4.18(7)	3.89(3)	0.011(2)	92.68(23)	1.09	0.93
HR67	31	72.45(23)	12.08(11)	1.03(3)	4.09(4)	3.91(3)	0.012(1)	93.59(23)	1.1	0.94
HR33	24	71.99(34)	13.20(31)	1.03(2)	4.20(6)	3.98(3)	0.0039(11)	94.40(49)	1.18	1.01
HR26	23	71.94(33)	12.16(15)	1.01(4)	4.15(8)	3.96(4)	0.0074(19)	93.23(18)	1.09	0.94
HR55	25	72.03(12)	12.26(6)	1.03(1)	4.10(5)	3.96(2)	0.0061(11)	93.39(15)	1.11	0.95
HR39	20	71.43(49)	12.22(17)	0.99(1)	4.29(7)	3.96(5)	0.0086(10)	92.97(57)	1.08	0.93
HR68	31	72.12(18)	12.23(11)	1.03(17)	4.20(6)	3.99(4)	0.011(1)	93.59(21)	1.09	0.93
HR37	21	70.83(32)	12.52(6)	1.07(2)	4.30(5)	4.03(4)	0.0073(13)	92.86(34)	1.09	0.94
HR40	8	71.16(34)	12.55(9)	1.05(2)	4.43(6)	4.00(5)	0.0093(9)	93.27(38)	1.08	0.93
HR43	11	70.69(15)	12.44(7)	1.03(1)	4.29(7)	4.04(3)	0.011(1)	92.55(12)	1.09	0.94
HR69	31	71.81(18)	12.51(10)	1.07(3)	4.25(6)	4.02(3)	0.012(1)	93.68(14)	1.1	0.94
HR38	21	70.48(32)	12.63(9)	1.11(2)	4.33(6)	4.05(3)	0.0063(9)	92.68(36)	1.1	0.93
HR41	21	70.54(22)	12.60(5)	1.04(1)	4.36(5)	4.06(3)	0.0087(11)	92.68(24)	1.09	0.94
HR44	20	70.66(61)	12.65(11)	1.08(2)	4.15(21)	4.01(7)	0.011(1)	92.59(69)	1.13	0.96
HR62	22	72.43(25)	12.05(10)	0.89(2)	4.02(9)	3.90(5)	0.0047(10)	93.31(25)	1.11	0.97
HR70	30	72.65(45)	12.04(12)	0.88(2)	4.06(22)	3.88(6)	0.0086(11)	93.52(52)	1.11	0.96
HR75	12	71.66(29)	12.27(21)	0.88(5)	4.08(6)	4.01(7)	0.011(1)	92.90(16)	1.11	0.97
HR77	20	72.01(39)	11.89(8)	0.86(3)	3.88(8)	3.84(7)	0.014(3)	92.52(49)	1.13	0.98
HR61	26	71.86(34)	12.27(11)	1.07(2)	4.08(9)	3.95(4)	0.0033(9)	93.23(32)	1.12	0.95
HR71	31	71.91(25)	12.37(7)	1.28(3)	4.14(7)	3.89(4)	0.0084(13)	93.61(35)	1.12	0.93
HR76	15	71.61(33)	12.19(12)	1.02(2)	4.03(6)	3.96(4)	0.010(1)	92.82(37)	1.12	0.95
HR78	19	71.12(44)	12.40(13)	1.09(4)	4.03(10)	3.90(5)	0.014(1)	92.59(49)	1.14	0.97

Notes: *Number of electron microprobe analyses ; **molar $Al_2O_3/(Na_2O+K_2O)$ ratio of the glasses; §molar $Al_2O_3/(CaO+Na_2O+K_2O)$ ratio of the glasses numbers in parentheses are one standard deviation in the last digit.

Table 4. Fluid/melt partitioning of sulfur at 2 kbar and 850 ˚C

Run no.	S in fluid (wt.%)	S in melt (wt.%)
	Co-CoO buffer, 0.85 wt.% bulk CaO	
HR62	3	0.0051 (12)
HR70	4.35	0.0079 (10)
HR75	5.61	0.011 (1)
HR77	7.01	0.014 (3)
	Co-CoO buffer, 2.01 wt.% bulk CaO	
HR61	1.55	0.0033 (9)
HR71	4.35	0.0084 (13)
HR76	5.61	0.010 (1)
HR78	7.01	0.014 (1)
	Ni-NiO buffer, 0.85 wt.% bulk CaO	
HR31	1.55	0.0051 (10)
HR36	3	0.0082 (19)
HR27	4.35	0.0098 (9)
HR34	5.61	0.010 (1)
HR66	7.01	0.010 (1)
	Ni-NiO buffer, 2.01 wt.% bulk CaO	
HR32	1.55	0.0042 (9)
HR25	3	0.0072 (19)
HR54	3	0.0065 (15)
HR28	4.35	0.011 (1)
HR35	5.61	0.011 (2)
HR67	7.01	0.012 (1)
	Ni-NiO buffer, 2.79 wt.% bulk CaO	
HR33	1.55	0.0041 (12)
HR26	3	0.0074 (19)
HR55	3	0.0061 (11)
HR39	4.35	0.0086 (10)
HR68	7.01	0.010 (1)
	Ni-NiO buffer, 3.98 wt.% bulk CaO	
HR37	3	0.0073 (13)
HR40	4.35	0.0092 (8)
HR43	5.61	0.011 (1)
HR69	7.01	0.012 (1)
	Ni-NiO buffer, 4.79 wt.% bulk CaO	
HR38	3	0.0063 (9)

HR41	4.35	0.0087 (11)
HR44	5.61	0.011 (1)
	Ni-NiO + 0.5 (unbuffered), 0.85 wt.% bulk CaO	
HR10	1.19 (4)	0.012 (1)
HR18	2.53 (3)	0.026 (1)
HR01	3.97 (3)	0.019 (1)
HR08	5.28 (3)	0.015 (1)
HR03	6.65 (3)	0.021 (1)
	Ni-NiO +0.5 (unbuffered), 2.01 wt.% bulk CaO	
HR19	0.55 (3)	0.010 (1)
HR17	1.91 (3)	0.015 (2)
HR29	3.08 (3)	0.036 (2)
HR20	4.40 (3)	0.068 (3)
HR84	4.58 (3)	0.031 (2)
HR05	5.98 (2)	0.047 (1)
HR79	5.95 (3)	0.038 (4)
	Ni-NiO +0.5 (unbuffered), 2.79 wt.% bulk CaO	
HR30	1.27 (5)	0.019 (1)
HR16	2.83 (3)	0.018 (1)
HR21	4.04 (3)	0.064 (6)
HR85	4.10 (3)	0.031 (3)
HR06	5.59 (3)	0.045 (2)
HR80	5.48 (3)	0.035 (2)
	Ni-NiO +0.5 (unbuffered) 4.79 wt.% bulk CaO	
HR02	1.87 (8)	0.013 (1)
HR07	3.18 (4)	0.013 (1)
HR04	4.64 (4)	0.015 (2)
	Re-ReO_2 buffer, 0.85 wt.% bulk CaO	
HR60	1.18 (3)	0.013 (1)
HR73	5.17 (4)	0.032 (4)

Notes: "Ni-NiO + 0.5" refers to an oxygen fugacity 0.5 to 1 log units above the Ni-NiO buffer. Errors are given in brackets (±1σ). For runs without anhydrite crystallization, the sulfur content of the fluid is assumed to be equal to that of the standard solution and no error is given.

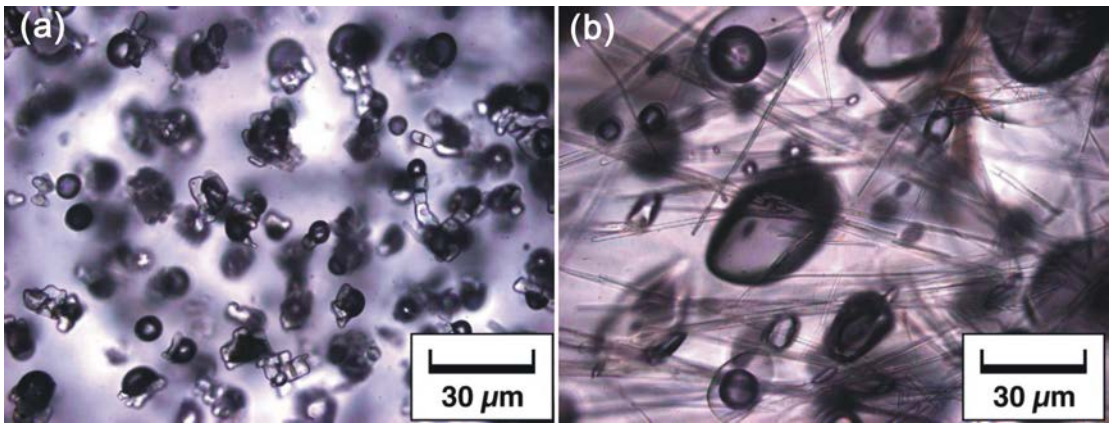

FIGURE 1. Images of run products as seen in transmitted light under a microscope. (a) Unbuffered experiment HR 29, showing blocky crystals of anhydrite together with dark fluid inclusions in a glass matrix; (b) experiment HR61 at the Co-CoO buffer, showing needles of wollastonite together with two-phase fluid inclusions in a glass matrix.

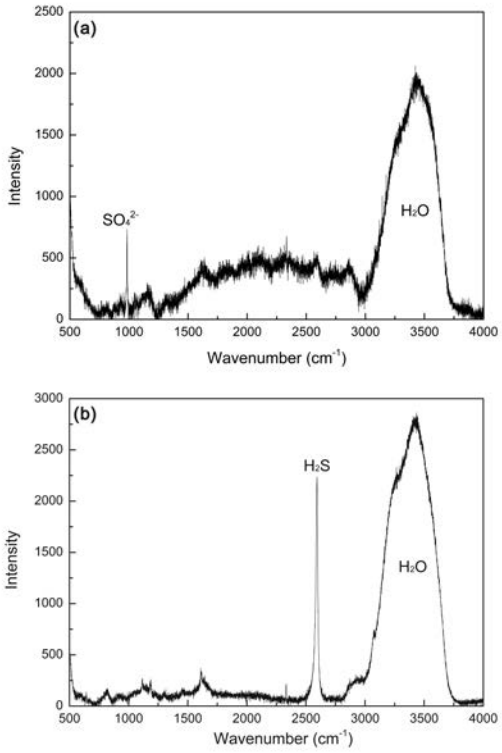

FIGURE 2. Raman spectra of the liquid phase of fluid inclusions in quenched glasses (a) unbuffered experiment HR08, (b) experiment HR27, buffered at Ni-NiO.

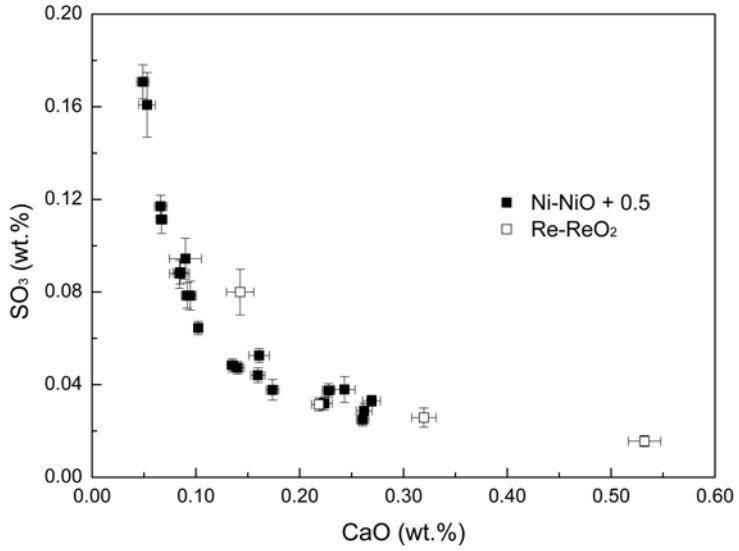

FIGURE 3. Inverse correlation between SO_3 and CaO contents in silicate melts coexisting with anhydrite at 850 ˚C and 2 kbar. Ni-NiO + 0.5 refers to an oxygen fugacity 0.5 to 1 log unit above the Ni-NiO buffer. Errors (1σ) are from microprobe measurements.

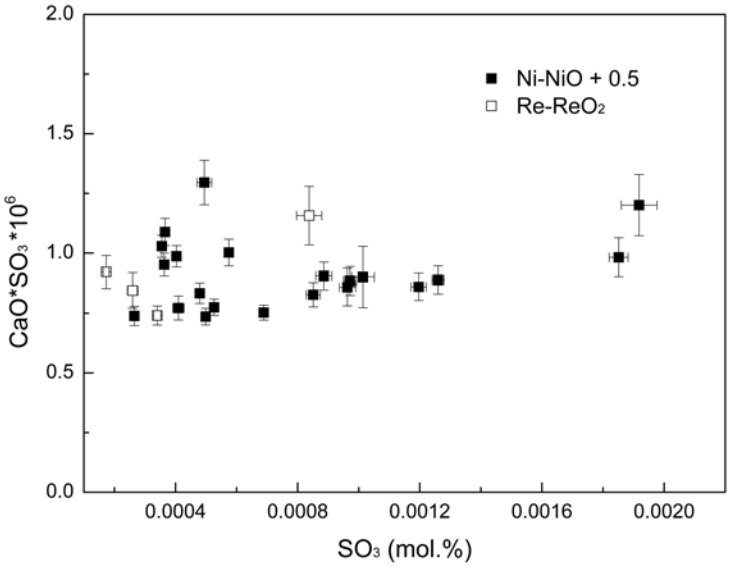

FIGURE 4. Solubility product [CaO][SO_3] (in molar fractions) in silicate melts coexisting with anhydrite. All data are from experiments at 850 ˚C and 2 kbar. Ni-NiO + 0.5 refers to an oxygen fugacity 0.5 to 1 log unit above the Ni-NiO buffer. Errors (1σ) are from microprobe measurements.

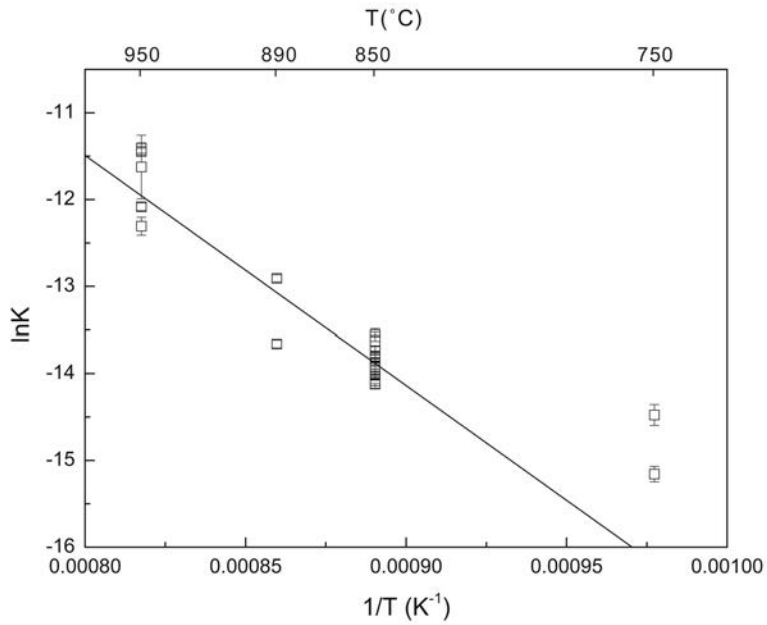

FIGURE 5. Temperature dependence of anhydrite solubility at 2 kbar and 750 – 950 ˚C. K is the solubility product $[CaO][SO_3]$ (in molar fractions).

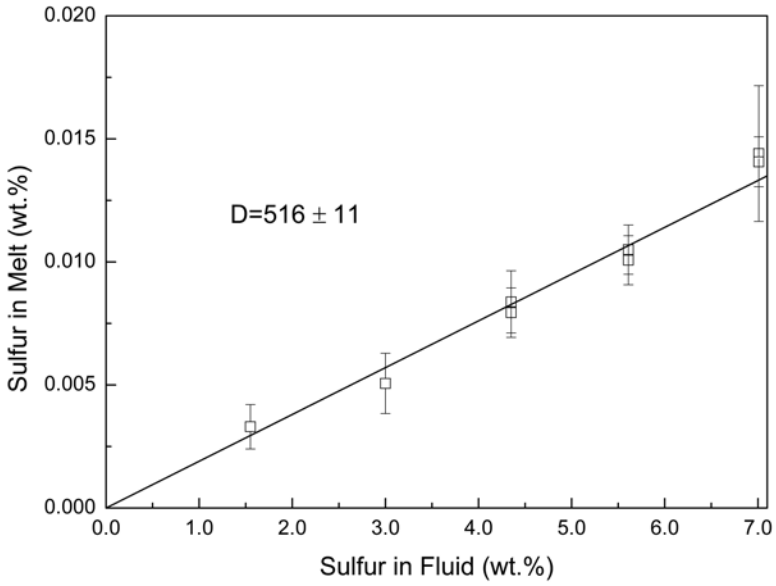

FIGURE 6. Distribution of sulfur between fluid and melt at 2 kbar, 850˚C and the Co-CoO buffer. The data can be described by a single fluid/melt partition coefficient. Runs for starting materials with different bulk CaO content are shown, but due to the crystallization of wollastonite, the quenched melts always contained about 1 wt. % of CaO.

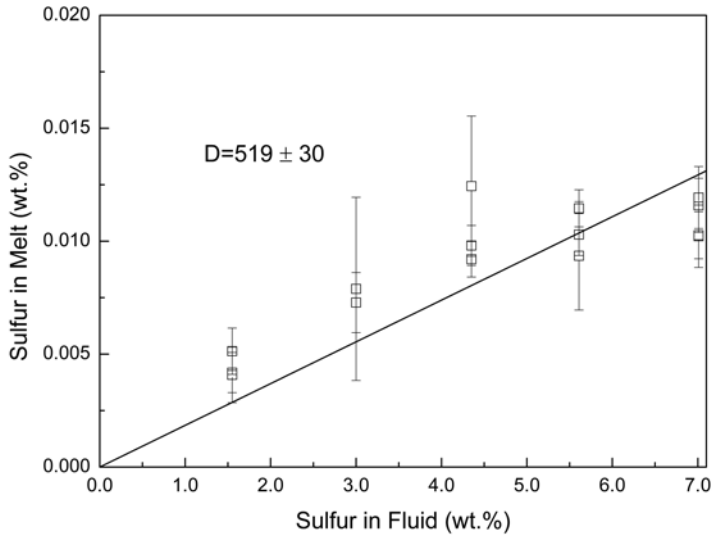

FIGURE 7. Distribution of sulfur between fluid and melt at 2 kbar, 850˚C and the Ni-NiO buffer. The data can be described by a single fluid/melt partition coefficient. Runs for starting materials with different bulk CaO content are shown, but due to the crystallization of wollastonite, the quenched melts always contained about 1 wt. % of CaO.

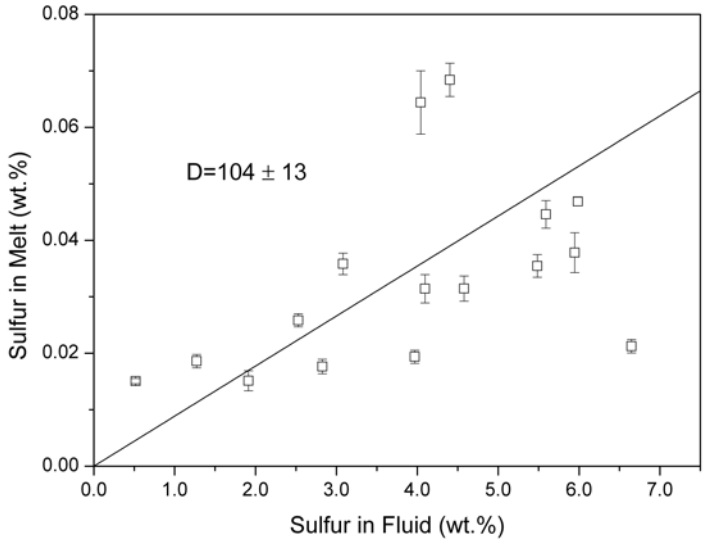

FIGURE 8. Distribution of sulfur between fluid and melt at 2 kbar, 850˚C and an oxygen fugacity 0.5 to 1 log unit above the Ni-NiO buffer, for experiments with less than 0.2 wt. % CaO in the quenched melt. The data can be described by a single fluid/melt partition coefficient.

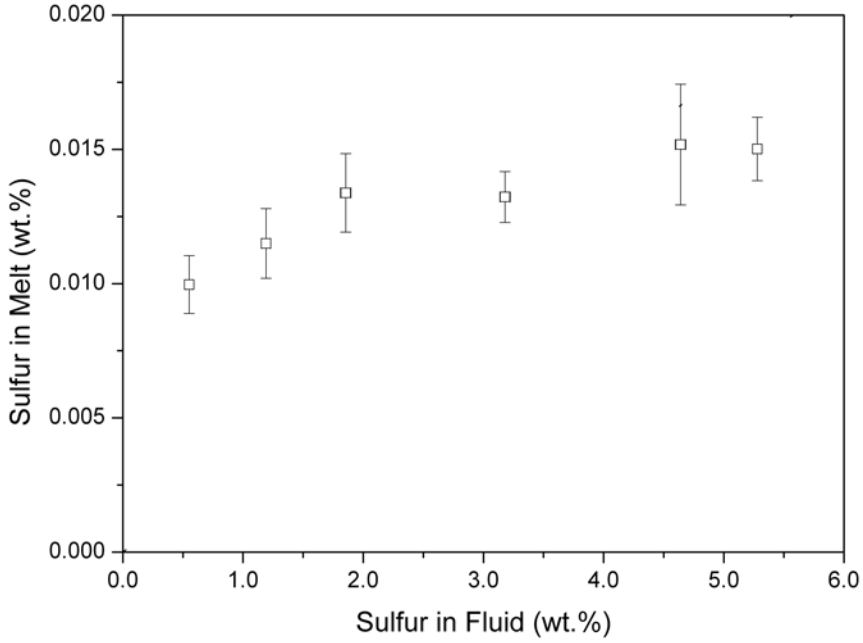

FIGURE 9. Distribution of sulfur between fluid and melt at 2 kbar, 850˚C and an oxygen fugacity 0.5 to 1 log unit above the Ni-NiO buffer, for experiments with more than 0.2 wt. % CaO in the quenched melt.

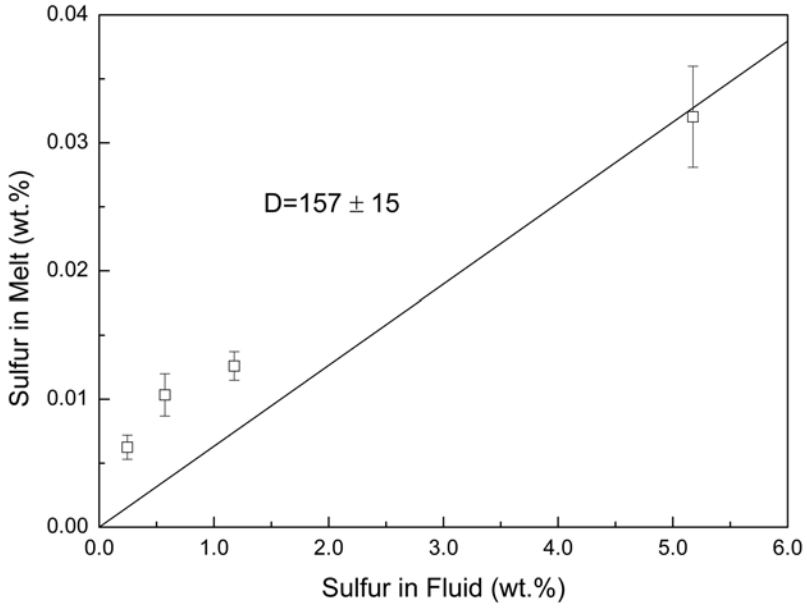

FIGURE 10. Distribution of sulfur between fluid and melt at 2 kbar, 850˚C and the Re-ReO_2 buffer. The data can be described by a single fluid/melt partition coefficient.

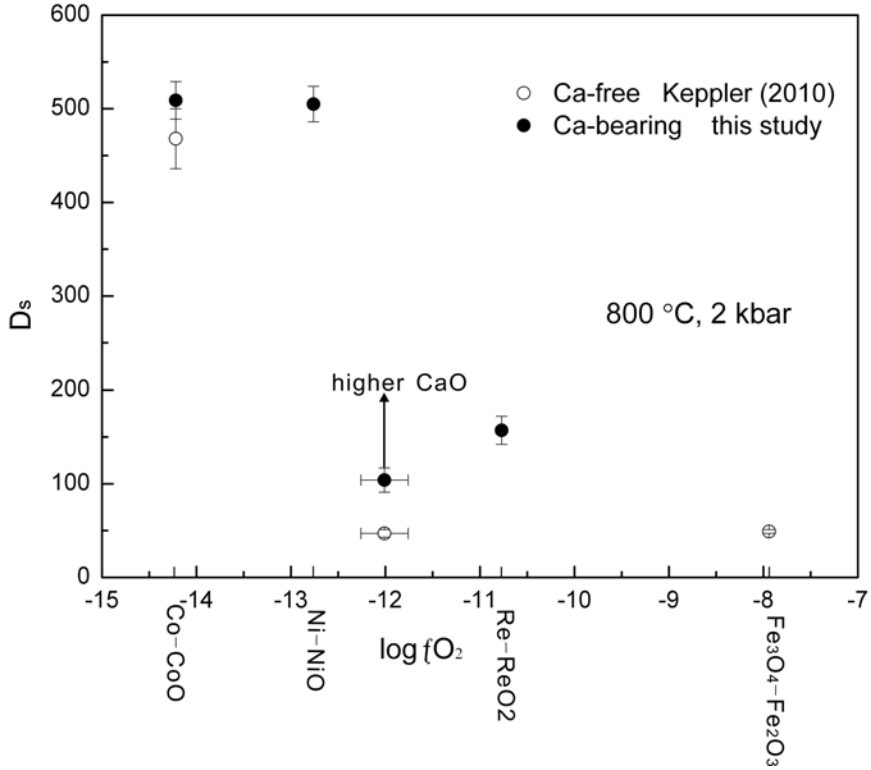

FIGURE 11. Dependence of the fluid/melt partition coefficient of sulfur on oxygen fugacity at 2 kbar, 850 ˚C. Data for the Ca-free haplogranite system are from Keppler (2010), the data for the haplogranite system with added CaO are from the present study. Note that the effect of CaO on partition coefficients seen under oxidizing condition (above the Ni-NiO buffer) may also be related to the peraluminous composition of the melts. See text for further discussion.

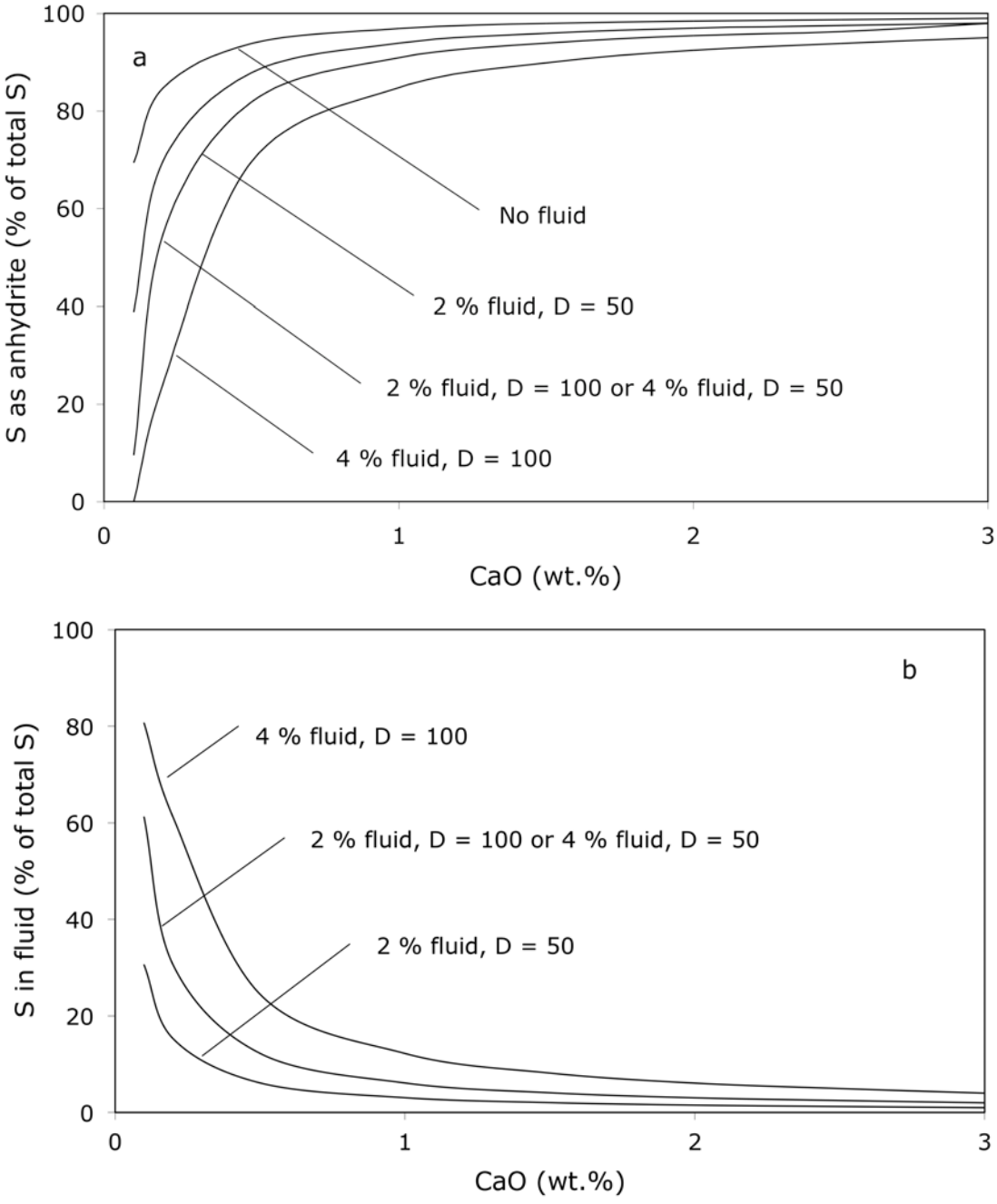

FIGURE 12. Effect of calcium on the behavior of sulfur in felsic melts under oxidizing conditions. The calculations assume a bulk concentration of sulfur in the system of 1000 ppm (equivalent to 2500 ppm SO_3), which is assumed to be completely in the S^{6+} state in the melt. D is the fluid/melt partition coefficient of sulfur.